Controlling the dewetting morphologies of thin liquid films by switchable substrates

S. Zitz [1,2,3,*] A. Scagliarini,[4,5,†] and J. Harting [1,6,‡]

[1]*Helmholtz Institute Erlangen-Nürnberg for Renewable Energy, Forschungszentrum Jülich, Fürther Strasse 248, D-90429 Nürnberg, Germany*
[2]*Department of Chemical and Biological Engineering, Friedrich-Alexander-Universität Erlangen-Nürnberg, Fürther Straße 248, D-90429 Nürnberg, Germany*
[3]*IMFUFA, Department of Science and Environment, Roskilde University, Postbox 260, DK-4000 Roskilde, Denmark*
[4]*Institute for Applied Mathematics "M. Picone" (IAC), Consiglio Nazionale delle Ricerche (CNR), Via dei Taurini 19, I-00185 Rome, Italy*
[5]*INFN, Sezione Roma "Tor Vergata", via della Ricerca Scientifica 1, I-00133 Rome, Italy*
[6]*Department of Chemical and Biological Engineering and Department of Physics, Friedrich-Alexander-Universität Erlangen-Nürnberg, Fürther Straße 248, D-90429 Nürnberg, Germany*

Switchable and adaptive substrates emerged as valuable tools for controlling wetting and actuation of droplet motion. Here, we report a computational study of the dynamics of an unstable thin liquid film deposited on a switchable substrate, modeled with a space- and time-varying contact angle. For a sufficiently large rate of wettability variation, a topological transition appears. Instead of breaking up into droplets, as expected for a substrate with multiple wetting minima, a metastable rivulet state emerges. A criterion discriminating whether or not rivulets occur is identified in terms of a single dimensionless parameter. Finally, we show and derive theoretically how the film rupture times, droplet shape, and rivulet lifetime depend on the pattern wavelength and speed.

Introduction. Wet surfaces and droplets are part of our everyday experience and of numerous industrial processes including coating, tribology, painting, and printing, to name but a few [1–6]. Moreover, the continuously growing interest for lab-on-a-chip devices [7,8] as well as for printable electronics or printable photovoltaics [9,10], whose efficiency relies crucially on a precise control of material deposition upon (de)wetting of liquid films, drew the attention to applications where the substrate is adaptive or switchable, i.e., it is not inert but responds dynamically to external stimuli or to the evolution of the coating liquid film itself [11]. Several realizations of switchable and adaptive substrates have been proposed [12], involving smart materials such as polymer brushes [13], thermal-responsive hydrogels [14], light-responsive molecules and microstructures [15], or processes such as electrowetting [16]. Modeling the coupled problem of a thin film on a switchable substrate and as such the dynamics of the substrate as well as the film is far from being trivial but can be realized by a space- and time-dependent wettability pattern [17]. While a consistent body

---

*zitz@ruc.dk
†andrea.scagliarini@cnr.it
‡j.harting@fz-juelich.de

of theoretical/computational work was devoted to processes on static heterogeneous substrates, the time-dependent case is still almost unexplored, with few exceptions focusing on single droplet spreading and sliding [17–19] or limited to analyzing the linear regime [20].

Here, we study by means of numerical simulations the full dewetting dynamics of a thin liquid film deposited on a substrate with a time-varying wettability pattern, starting from a slightly perturbed film to film rupture and long-time morphology [21]. We identify two regimes where the rupture times grow with the pattern wavelength either linearly (on a static pattern) or attain a constant value (in the time-dependent case), for short wavelengths, and approach a quadratic law as the wavelength increases. These observations are then explained theoretically. We show that, by tuning the rate of change of the underlying pattern, one can control the dewetting morphology, which is often desired in microfluidic applications. In particular, for large enough pattern speeds, we detect a state where the film retracts into metastable rivulets, eventually breaking up into multiple droplets. We introduce a control parameter to discriminate whether rivulets or just droplets (as in the static situation) can be observed and propose a phenomenological argument to justify the logarithmic dependence of the rivulets' lifetime on the pattern speed.

Method. In order to simulate the dewetting dynamics on patterned, "switchable," substrates, we integrate numerically the thin-film equation [22,23]

$$\partial_t h(\mathbf{x}, t) = \nabla \cdot [M_\delta(h)\nabla p(\mathbf{x}, t)] \tag{1}$$

by means of a recently developed lattice Boltzmann (LB) scheme [24–26]. Equation (1) describes, in a lubrication approximation spirit, the evolution of the height field (film thickness) $h(\mathbf{x}, t)$, denoting the location of the liquid/gas interface. The mobility function $M_\delta(h) = \frac{2h^3 + 6\delta h^2 + 3\delta^2 h}{6\mu}$ depends on the velocity boundary condition at the substrate, parametrized by an effective slip length δ (for $\delta \to 0$ it reduces to the no-slip form $h^3/(3\mu)$) [27–30]. Here, μ is the fluid dynamic viscosity. The film pressure $p(\mathbf{x}, t)$ consists of the sum of the Laplace and disjoining pressures, that is, $p(\mathbf{x}, t) = -\gamma\nabla^2 h - \Pi$ (γ is the surface tension [31]). The disjoining pressure Π can be seen as (minus) the derivative, with respect to the film thickness, of an effective interfacial potential [32]. As such, it contains the information on the liquid/solid and solid/gas interactions and, hence, on the wettability, which is parametrized in terms of the contact angle θ [33–36]. The expression adopted for Π is

$$\Pi(h, \theta) = \frac{2\gamma}{h_*}\{1 - \cos[\theta(\mathbf{x}, t)]\}f\left(\frac{h}{h_*}\right), \tag{2}$$

where $f(\xi) = \xi^{-3} - \xi^{-2}$. h_* is the height at which Π vanishes and sets the precursor layer thickness [34,37–39]. The time variation of the patterned substrate enters the model through the disjoining pressure, by making the contact angle space and time dependent, i.e., $\theta = \theta(\mathbf{x}, t)$. We decorate the substrate with a checkerboard pattern, a common choice that generalizes the broken homogeneity of the stripes to two directions [40–42]. In particular, we employ the sinusoidal form

$$\theta(\mathbf{x}, t) = \theta_0 + \delta\theta\{\sin[q_\theta(x + v_{\theta x}t)]\sin[q_\theta(y + v_{\theta y}t)]\}, \tag{3}$$

where $q_\theta = 2\pi/\lambda$, i.e., the pattern evolves in time as a plane wave. We fix the velocity direction to one diagonal, namely $\mathbf{v}_\theta = (v_{\theta x}, v_{\theta y}) = v_\theta(1/\sqrt{2}, -1/\sqrt{2})$ (we will return later to the importance of this choice), and we set $\theta_0 = 20°$ and $\delta\theta = 10°$ [43]. Length scales and timescales will be expressed, respectively, in units of the mean film height h_0 (which is constant in time, due to mass conservation), and of $t_0 = \frac{3\mu}{\gamma h_0^3 q_0^4}$, the inverse growth rate of the most unstable mode, whose wave number is q_0, of a spinodally dewetting film [44]. On a uniform substrate, with constant contact angle $\theta^{(u)}$, the wave number reads $(q_0^{(u)})^2 = h_*^{-2}(1 - \cos\theta^{(u)})f'(h_0/h_*)$ [44,45]. In our patterned case, we define $q_0^2 = h_*^{-2}(1 - \cos\theta_0)f'(h_0/h_*)$. Correspondingly, we choose as a velocity scale $v_0 = \lambda_s/t_0$, where $\lambda_s = 2\pi/q_0$. Figure 1 shows $h(\mathbf{x}, t)$ (droplets) and $\theta(\mathbf{x})$ (color coded) for $v_\theta = 0$ (i.e., the static case) and $\lambda = 256h_0$ [46], in the late stages of dewetting. As expected, droplets form in regions of small contact angles (blue) while the regions of high contact angles (yellow) dewet.
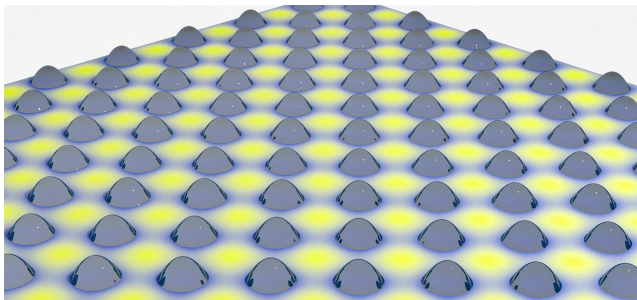
FIG. 1. Stationary film thickness field ($t > t_0$) showing the formation of droplets. The color map indicates the contact angle pattern (Eq. (3) with $v_\theta = 0$), with lower (higher) values in light blue (yellow).

Results. We first investigate how the rupture times depend on the parameters characterizing the wettability pattern, namely the wavelength of the contact angle variation λ and wave speed v_θ [47–51]. The film rupture time τ_r is defined as the least t such that $h(\mathbf{x}, \tau_r) = h_*$ (i.e., when the free surface "touches" the substrate). In Fig. 2 we report the rupture times as a function of the wavelength, for stationary ($v_\theta = 0$) and time-dependent ($v_\theta = 20v_0$) patterns. It is conveyed that, overall, rupture occurs earlier on the static substrate, suggesting that the time variation tends to stabilize the film, in agreement with linear stability analysis results [20]. We observe that τ_r grows linearly with λ for short wavelengths and quadratically for longer λ. These facts can be qualitatively explained as follows. In this case, from the linearized thin-film equation (in one spatial dimension, for simplicity), obtained setting $h = h_0 + \delta h$ with $\delta h \ll h_0$, we can easily see that the exponential growth of the height perturbation is affected by the wettability pattern (variable contact angle) in such a way that $\partial_t(\delta h) \propto \{\partial_x^2[\partial_h \Pi(h_0)]\}\delta h$. Therefore, since the characteristic time t_θ can be estimated dimensionally as $t_\theta \sim \delta h/(\dot{\delta h})$, the rupture time should go as

$$\tau_r \sim t_\theta \sim \delta h/(\dot{\delta h}) \propto \frac{3\mu}{h_0^3}\{\partial_x^2[\partial_h \Pi(h_0)]\}^{-1} \sim t_0\left(\frac{q_\theta}{q_0}\right)^{-2} \propto t_0 q_0^2 \lambda^2. \quad (4)$$

Conversely, for fast growths ($t_\theta \ll t_R$), retraction dominates and fixes the timescale, $\tau_r \sim t_R$. The latter is related to the time the liquid takes to flow out of regions of high contact angle, whose size
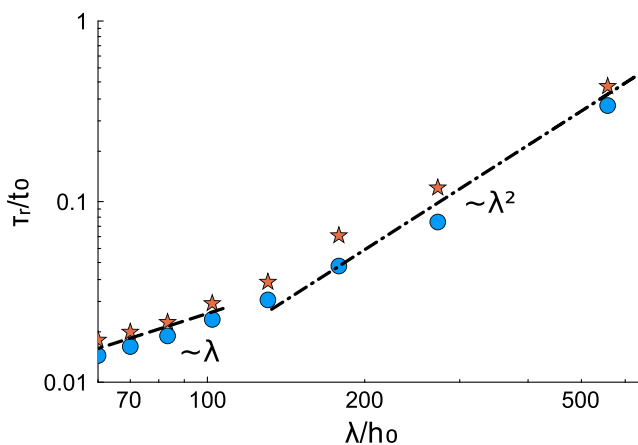
FIG. 2. Rupture times τ_r as a function of the pattern wavelength λ, for $v_\theta = 0$ ($\bullet$) and $v_\theta = 20v_0$ ($\star$). The continuous and dashed lines indicate the linear, $\sim\lambda$, and quadratic, $\sim\lambda^2$, scaling laws, respectively.
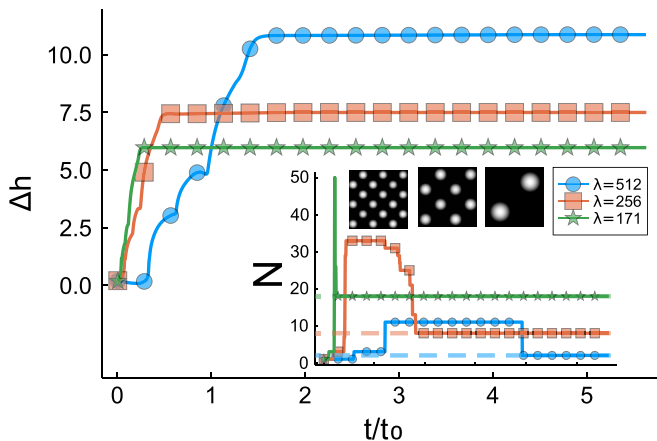
FIG. 3. Main panel: Time evolution of the height fluctuations $\Delta h(t)$ during the dewetting process on the patterned substrate given by Eq. (3) with $v_\theta = 0$ and $\lambda = 512h_0$ (•), $\lambda = 256h_0$ (■), and $\lambda = 170h_0$ (⋆). Inset: Number of droplets $N(t)$ as a function of time. The three horizontal dashed lines indicate the number of minima of Eq. (3), which is $2(\frac{L}{\lambda})^2$. The snapshots depict the stationary droplet states as grayscale images of the film thickness field $h(\mathbf{x}, t)$.

is $\sim\lambda$. Hence we have

$$\tau_r \sim \tau_R \propto U_\Theta^{-1}\lambda, \tag{5}$$

where U_Θ is the retraction speed $U_\Theta = \frac{\gamma\Theta^3}{9\mu}$ [52], with $\Theta = \max_{\mathbf{x}}\{\theta(\mathbf{x})\}$. We now focus on the long-time dynamics, the characterization of the dewetting morphologies, and how they are affected by the speed of the wettability wave. On the stationary substrate, after rupture all fluid accumulates in droplets centered at contact angle minima. Consequently, as seen from the inset of Fig. 3, where we plot the number of droplets $N(t)$ versus time [53], in the steady state ($t \gg t_0$) $N(t)$ attains the value $N_\infty = 2(L/\lambda)^2$ (horizontal lines), which equals the minima of Eq. (3), for $v_\theta = 0$. Notice that the number of droplets converges faster for smaller pattern wavelengths, in line with the observation reported and justified in the previous section that the characteristic dewetting time decreases with the wavelength.

In the main panel of the figure, the height fluctuations $\Delta h(t) = \max_{\mathbf{x}}\{h(\mathbf{x}, t)\} - \min_{\mathbf{x}}\{h(\mathbf{x}, t)\}$ grow in time until film rupture and then settle to a constant value. This represents a measure of the mean droplet height h_d (since droplets are essentially monodisperse), decreasing with the pattern wavelength (as expected, due to a decreasing droplet volume, $V_d = \frac{h_0\lambda^2}{2}$).

A time-dependent pattern affects the dewetting morphology quite substantially. For $v_\theta = 1.7v_0$ we still observe the formation of droplets, similarly to the stationary case ($v_\theta = 0$). However, these are transported with the contact angle minima, reproducing a somehow similar behavior recently described in a numerical study of a droplet on a moving wettability step [17]. If the pattern speed is further increased, for $v_\theta = 17.5v_0$ we observe the development of rivuletlike structures, aligned with $\mathbf{v}_\theta$. The film, in fact, while dewetting in the direction normal to the pattern velocity, is exposed, in the direction of the velocity, to a periodic potential with alternating minima and saddle points, which partially (as we will see) stabilizes the film over "preferential" lanes along the diagonals. This makes the chosen velocity direction, $(1/\sqrt{2}, -1/\sqrt{2})$ (or, equivalently, the orthogonal one $(1/\sqrt{2}, 1/\sqrt{2})$), optimal for the formation of rivulets.

In order to better characterize the various morphologies we apply the theory of Minkowski's functionals. In particular, we employ the second-order Minkowski structure metric q_2 [54,55], which can be computed from a Voronoi tessellation of the set of discrete points (x_i, y_i) on the two-dimensional (2D) lattice, such that the height field lies above a certain threshold [56]. The
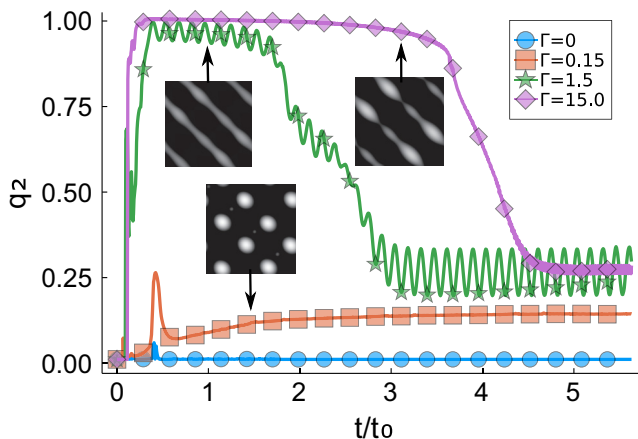
FIG. 4. Time evolution of the second-order Minkowski structure metric $q_2(t)$ for different Γ values, on a substrate with pattern wavelength $\lambda = 256h_0$. The grayscale insets supply snapshots of the corresponding film thickness fields.

q_2 metric quantifies the degree of anisotropy of the dewetting morphology, so it takes relatively large values if the structures formed display a preferential direction. Measuring q_2 then enables us to clearly distinguish between the formation of droplets and rivulets: Much larger q_2 values are attained for the latter type of structure, as we can see in Fig. 4. We observe, on the other hand, that such rivulets are metastable and eventually break up into droplets, as indicated by the collapse of q_2 at later times. Notice, though, that the q_2 signal for any $v_\theta > 0$ always stays above the one for the static case, suggesting that even the smallest pattern velocity introduces a sizable deformation of the spherical cap shape. The breakup is the result of a varicose mode of the rivulet [57,58], whose wavelength is $\approx \lambda$, such that only $N_\infty/2$ droplets are counted after breakup. These droplets show a peculiar dynamics, characterized by a periodic sequence of spreading and retraction, driven by the pattern, that we dub the "pumping state" [59].

We argue that the emergence of rivulets is controlled by the competition of two characteristic velocities, the pattern wave speed v_θ and the retraction speed U_Θ, introduced in Eq. (5). If U_Θ is large as compared to v_θ, the film retraction is faster than the local contact angle variation and thus droplets form. However, if v_θ is larger than U_Θ, then the retracting film has too little time to form droplets and ends up in the metastable rivulet state. It appears, therefore, natural to consider the ratio of these two velocities, $\Gamma \equiv v_\theta/U_\theta$, as the discriminating parameter. We see from Fig. 4 that indeed rivulets form only for $\Gamma > 1$. Moreover, the larger the Γ, the more stable are the rivulets; in other words, the rivulet lifetime τ_{riv}, that can be conventionally taken as the time at which the drop of q_2 occurs, grows with v_θ (see Fig. 5). The rivulet itself is, in fact, prone to dewetting, with the liquid accumulating over patches around contact angle minima. However, as the pattern moves, the instability is tamed due to configurations whereby higher contact angle regions underlie height field maxima, thus tending to revert the fluid flow. Heuristically speaking, this means that, if we evaluate $\Delta h(t)$ restricted on the rivulet axis, it should grow exponentially (with a certain growth rate $\alpha \propto t_0$) only when the system is in the unstable configuration. Namely, $\Delta h(t)/\Delta h_0 \propto e^{\alpha t}$ (see the inset of Fig. 5) with a prefactor proportional to the time spent by the rivulet in such a configuration, which goes as $\sim \lambda/v_\theta$, therefore $\Delta h(t)/\Delta h_0 \sim \alpha(\lambda/v_\theta)e^{\alpha t}$. The rivulet lifetime can be seen as the rupture time of the structure along its axis, hence such that $\Delta h(\tau_{\text{riv}}) \sim h_0$ [25], which yields

$$\tau_{\text{riv}} \sim \alpha \log(v_\theta) \propto t_0 \log(\Gamma). \tag{6}$$

This logarithmic dependence is indeed observed in the numerical data as shown in Fig. 5.
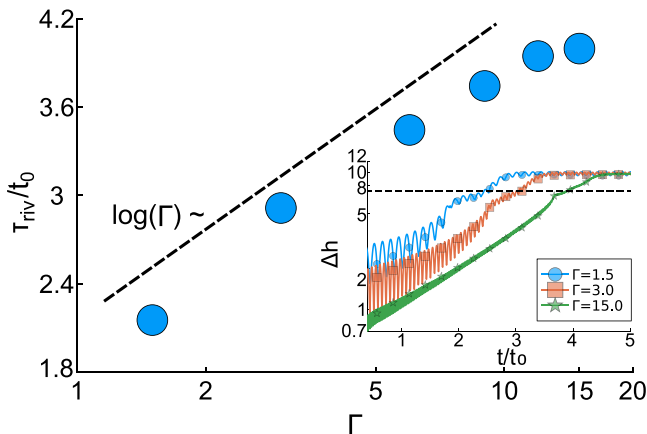
FIG. 5. Main panel: Rivulet lifetimes τ_{riv} for various Γ. The dashed line is a guide to the eye to highlight the logarithmic dependence, in agreement with the theoretical prediction, Eq. (6). Inset: Height fluctuations $\Delta h(t)$ vs time, along the rivulet axis, for three different Γ.

We envisage a possible realization of a dewetting experiment on a switchable substrate of the type modeled by the spatiotemporal contact angle (3). One may think of a thin liquid film cast on a light responsive substrate [15], under the action of controlled external stimuli (a light emitter). An ideal candidate could be a digital multimirror device (DMD). This technology was effectively used for thin-film experiments and additive manufacturing [60,61]. It allows for fast temporal modulations of the optical signal (with frequencies up to ≈ 16 kHz) with a spatial resolution of $\approx 10 \times 10$ μm^2 (the size of a pixel). Considering as a reference, for instance, the system studied in Refs. [62,63], namely a $\sim$4-nm-thick film of polystyrene deposited on an oxidized silicon wafer, we evaluate the retraction speed $U_{\Theta} = \frac{\Theta^3 \gamma}{9\mu}$ to be $U_{\Theta} \approx 10^{-2}$ μm/s. The (minimum) *pattern speed* can be estimated from the pixel size with frame rate ~ 1 s^{-1} as $v_{\theta} \sim 10$ μm/s, which would result in $\Gamma \sim 10^3$, i.e., well within the rivulet regime ($\Gamma > 1$). Also, both U_{Θ} and v_{θ} can be widely modulated, the former by varying the (temperature- and molecular-weight-dependent) viscosity or tailoring the substrate to make it more hydrophobic (i.e., increasing the contact angle), and the latter by tuning the spatial resolution and frame rate of the DMD. Thus, we expect the range of achievable Γ's to be feasibly extended both to very high ($\Gamma \gg 1$) and very low ($\Gamma \ll 1$) values.

Conclusions. We presented numerical simulations and a theoretical analysis on the dewetting of thin liquid films on a switchable substrate. Studying how the film stability depends on the underlying static pattern, we found that the rupture times grow linearly with the pattern wavelength, for short wavelengths, and quadratically in the long-wavelength limit. In the time-dependent case, the rupture times are generally longer, indicating an induced greater film stability, and, while the quadratic growth is preserved at long wavelengths, a plateauing behavior was observed as the wavelength decreases. Furthermore, we showed that, at increasing the wettability wave speed, a transition occurs in the dewetting morphology from a multidroplet to a metastable multirivulet state. We find that this surprising morphological transition can be described with a single dimensionless parameter Γ. Considering only the ratio of the pattern speed and the typical film retraction speed, the rivulets' lifetime itself grows with the pattern speed, displaying a logarithmic dependence that was captured by means of phenomenological arguments. On a broader perspective, our work suggests that switchable substrates offer another avenue to control thin-film dewetting, with obviously relevant implications, for instance, for open microfluidic devices, and paves the way to future studies in this direction, exploiting more complex and dedicated space-time dependencies.

[1] W. A. Gross, L. A. Matsch, V. Castelli, A. Eshel, J. H. Vohr, and M. Wildmann, *Fluid Film Lubrication* (Wiley, New York, 1980).

[2] A. Z. Szeri, *Fluid Film Lubrication*, 2nd ed. (Cambridge University Press, Cambridge, UK, 2010).

[3] D. Quéré, Fluid coating on a fiber, Annu. Rev. Fluid Mech. **31**, 347 (1999).

[4] A. S. da Silva Sobrinho, G. Czeremuszkin, M. Latrèche, G. Dennler, and M. R. Wertheimer, A study of defects in ultra-thin transparent coatings on polymers, Surf. Coat. Technol. **116-119**, 1204 (1999).

[5] M. Singh, H. M. Haverinen, P. Dhagat, and G. E. Jabbour, Inkjet printing—process and its applications, Adv. Mater. **22**, 673 (2010).

[6] H. Wijshoff, The dynamics of the piezo inkjet printhead operation, Phys. Rep. **491**, 77 (2010).

[7] E. Samiei, M. Tabrizian, and M. Hoorfar, A review of digital microfluidics as portable platforms for lab-on a-chip applications, Lab Chip **16**, 2376 (2016).

[8] M. Focke, D. Kosse, C. Müller, H. Reinecke, R. Zengerle, and F. von Stetten, Lab-on-a-foil: Microfluidics on thin and flexible films, Lab Chip **10**, 1365 (2010).

[9] N. A. Luechinger, E. K. Athanassiou, and W. J. Stark, Graphene-stabilized copper nanoparticles as an air-stable substitute for silver and gold in low-cost ink-jet printable electronics, Nanotechnology **19**, 445201 (2008).

[10] O. J. J. Ronsin and J. Harting, Formation of crystalline bulk heterojunctions in organic solar cells: Insights from phase-field simulations, ACS Appl. Mater. Interfaces **14**, 49785 (2022).

[11] H.-J. Butt, R. Berger, W. Steffen, D. Vollmer, and S. A. L. Weber, Adaptive wetting—adaptation in wetting, Langmuir **34**, 11292 (2018).

[12] B. Xin and J. Hao, Reversibly switchable wettability, Chem. Soc. Rev. **39**, 769 (2010).

[13] M. A. C. Stuart, W. T. S. Huck, J. Genzer, M. Müller, C. Ober, M. Stamm, G. B. Sukhorukov, I. Szleifer, V. V. Tsukruk, M. Urban, F. Winnik, S. Zauscher, I. Luzinov, and S. Minko, Emerging applications of stimuli-responsive polymer materials, Nat. Mater. **9**, 101 (2010).

[14] L. Chen, M. Liu, L. Lin, T. Zhang, J. Ma, Y. Song, and L. Jiang, Thermal-responsive hydrogel surface: Tunable wettability and adhesion to oil at the water/solid interface, Soft Matter **6**, 2708 (2010).

[15] K. Ichimura, S.-K. Oh, and M. Nakagawa, Light-driven motion of liquids on a photoresponsive surface, Science **288**, 1624 (2000).

[16] F. Mugele, A. Klingner, J. Buehrle, D. Steinhauser, and S. Herminghaus, Electrowetting: A convenient way to switchable wettability patterns, J. Phys.: Condens. Matter **17**, S559 (2005).

[17] J. Grawitter and H. Stark, Steering droplets on substrates using moving steps in wettability, Soft Matter **17**, 2454 (2021).

[18] J. Grawitter and H. Stark, Droplets on substrates with oscillating wettability, Soft Matter **17**, 9469 (2021).

[19] U. Thiele and S. Hartmann, Gradient dynamics model for drops spreading on polymer brushes, Eur. Phys. J. Spec. Top. **229**, 1819 (2020).

[20] B. Suman and S. Kumar, Dynamics of thin liquid films on surfaces with a time-periodic wettability, J. Colloid Interface Sci. **304**, 208 (2006).

[21] R. Konnur, K. Kargupta, and A. Sharma, Instability and morphology of thin liquid films on chemically heterogeneous substrates, Phys. Rev. Lett. **84**, 931 (2000).

[22] A. Oron, S. H. Davis, and S. G. Bankoff, Long-scale evolution of thin liquid films, Rev. Mod. Phys. **69**, 931 (1997).

[23] R. V. Craster and O. K. Matar, Dynamics and stability of thin liquid films, Rev. Mod. Phys. **81**, 1131 (2009).

[24] S. Zitz, A. Scagliarini, S. Maddu, A. A. Darhuber, and J. Harting, Lattice Boltzmann method for thin-liquid-film hydrodynamics, Phys. Rev. E **100**, 033313 (2019).

[25] S. Zitz, A. Scagliarini, and J. Harting, Lattice Boltzmann simulations of stochastic thin film dewetting, Phys. Rev. E **104**, 034801 (2021).

[26] S. Zitz, M. Zellhöfer, A. Scagliarini, and J. Harting, Swalbe.jl: A lattice Boltzmann solver for thin film hydrodynamics, J. Open Source Softw. **7**, 4312 (2022).

[27] C. Huh and L. E Scriven, Hydrodynamic model of steady movement of a solid/liquid/fluid contact line, J. Colloid Interface Sci. **35**, 85 (1971).

[28] D. Peschka, S. Haefner, L. Marquant, K. Jacobs, A. Münch, and B. Wagner, Signatures of slip in dewetting polymer films, Proc. Natl. Acad. Sci. USA **116**, 9275 (2019).

[29] R. Fetzer, A. Münch, B. Wagner, M. Rauscher, and K. Jacobs, Quantifying hydrodynamic slip: A comprehensive analysis of dewetting profiles, Langmuir **23**, 10559 (2007).

[30] A. Münch, B. A. Wagner, and T. P. Witelski, Lubrication models with small to large slip lengths, J. Eng. Math. **53**, 359 (2005).

[31] Y. Wu, F. Wang, S. Ma, M. Selzer, and B. Nestler, How do chemical patterns affect equilibrium droplet shapes? Soft Matter **16**, 6115 (2020).

[32] B. V. Deryaguin and N. V. Churaev, On the question of determining the concept of disjoining pressure and its role in the equilibrium and flow of thin films, J. Colloid Interface Sci. **66**, 389 (1978).

[33] D. Bonn, J. Eggers, J. Indekeu, J. Meunier, and E. Rolley, Wetting and spreading, Rev. Mod. Phys. **81**, 739 (2009).

[34] L. W. Schwartz and R. R. Eley, Simulation of droplet motion on low-energy and heterogeneous surfaces, J. Colloid Interface Sci. **202**, 173 (1998).

[35] T. Young, III. An essay on the cohesion of fluids, Philos. Trans. R. Soc. London **95**, 65 (1805).

[36] P. G. de Gennes, Wetting: Statics and dynamics, Rev. Mod. Phys. **57**, 827 (1985).

[37] See Supplemental Material at http://link.aps.org/supplemental/10.1103/PhysRevFluids.8.L122001 for the disjoining pressure and compare our findings to a relevant experiment. In addition, we supply further details about the Minkovski functional q_2 and some theoretical derivation for the emergence of the observed interface shapes.

[38] V. S. Mitlin, Dewetting of solid surface: Analogy with spinodal decomposition, J. Colloid Interface Sci. **156**, 491 (1993).

[39] G. F. Teletzke, H. T. Davis, and L. E. Scriven, How liquids spread on solids, Chem. Eng. Commun. **55**, 41 (1987).

[40] M. Jalali, A. R. White, J. Marti, and J. Sheng, Fabrication and characterization of a scalable surface textured with pico-liter oil drops for mechanistic studies of bacteria-oil interactions, Sci. Rep. **8**, 7612 (2018).

[41] G. Nagayama and D. Zhang, Intermediate wetting state at nano/microstructured surfaces, Soft Matter **16**, 3514 (2020).

[42] P. Das, P. K. Jaiswal, and S. Puri, Surface-directed spinodal decomposition on chemically patterned substrates, Phys. Rev. E **102**, 012803 (2020).

[43] Since a typical velocity is such that $v_\theta \Delta t \ll \Delta x$ (in one time step Δt the wave would travel a distance much smaller than a lattice spacing Δx), the time update needs to be interpreted in an integer part sense, that is, the pattern is shifted by Δx every $1/v_{\theta x}\Delta t$ (equivalently in the y direction).

[44] K. Mecke and M. Rauscher, On thermal fluctuations in thin film flow, J. Phys.: Condens. Matter **17**, S3515 (2005).

[45] Y. Zhang, J. E. Sprittles, and D. A. Lockerby, Molecular simulation of thin liquid films: Thermal fluctuations and instability, Phys. Rev. E **100**, 023108 (2019).

[46] For a better visualization double the domain length L and periodically continue the image.

[47] K. Kargupta and A. Sharma, Morphological self-organization by dewetting in thin films on chemically patterned substrates, J. Chem. Phys. **116**, 3042 (2002).

[48] K. Kargupta, R. Konnur, and A. Sharma, Instability and pattern formation in thin liquid films on chemically heterogeneous substrates, Langmuir **16**, 10243 (2000).

[49] G. Nisato, B. D. Ermi, J. F. Douglas, and A. Karim, Excitation of surface deformation modes of a phase-separating polymer blend on a patterned substrate, Macromolecules **32**, 2356 (1999).

[50] A. Karim, J. F. Douglas, B. P. Lee, S. C. Glotzer, J. A. Rogers, R. J. Jackman, E. J. Amis, and G. M. Whitesides, Phase separation of ultrathin polymer-blend films on patterned substrates, Phys. Rev. E **57**, R6273(R) (1998).

[51] S. Succi, *The Lattice Boltzmann Equation: For Fluid Dynamics and Beyond* (Clarendon Press, Oxford, UK, 2001).

[52] A. M. J. Edwards, R. Ledesma-Aguilar, M. I. Newton, C. V. Brown, and G. McHale, Not spreading in reverse: The dewetting of a liquid film into a single drop, Sci. Adv. **2**, e1600183 (2016).

[53] A droplet is identified by the set ("cluster") of points, in the plane, constituting each of the connected components of the set $\{\mathbf{x} \in [0, L]^2 | h(\mathbf{x}, t) \geqslant h_*\}$.

[54] W. Mickel, S. C. Kapfer, G. E. Schröder-Turk, and K. Mecke, Shortcomings of the bond orientational order parameters for the analysis of disordered particulate matter, J. Chem. Phys. **138**, 044501 (2013).

[55] F. M. Schaller, J. Wagner, and S. C. Kapfer, Papaya2: 2D irreducible Minkowski tensor computation, J. Open Source Softw. **5**, 2538 (2020).

[56] The expression is $q_2 = \frac{1}{N} \sum_j \frac{1}{P_j} | \sum_k L_k^{(j)} e^{2i\phi_k^{(j)}} |$, where the inner sum runs over the edges of length $L_k^{(j)}$, of the jth Voronoi cell, whose perimeter is P_j, and $\phi_k^{(j)}$ is the polar angle of the normal to the kth edge. The outer sum represents an ensemble average over the N points in the set.

[57] J. A. Diez, A. G. González, and L. Kondic, On the breakup of fluid rivulets, Phys. Fluids **21**, 082105 (2009).

[58] S. Mechkov, M. Rauscher, and S. Dietrich, Stability of liquid ridges on chemical micro- and nanostripes, Phys. Rev. E **77**, 061605 (2008).

[59] See movie ligament_formation_and_breakup.mp4 in the Supplemental Material [37].

[60] J. A. Vieyra Salas, J. M. van der Veen, J. J. Michels, and A. A. Darhuber, Active control of evaporative solution deposition by modulated infrared illumination, J. Phys. Chem. C **116**, 12038 (2012).

[61] S. K. Saha, D. Wang, V. H. Nguyen, Y. Chang, J. S. Oakdale, and S.-C. Chen, Scalable submicrometer additive manufacturing, Science **366**, 105 (2019).

[62] J. Becker, G. Grün, R. Seemann, H. Mantz, K. Jacobs, K. R. Mecke, and R. Blossey, Complex dewetting scenarios captured by thin-film models, Nat. Mater. **2**, 59 (2003).

[63] R. Fetzer, M. Rauscher, R. Seemann, K. Jacobs, and K. Mecke, Thermal noise influences fluid flow in thin films during spinodal dewetting, Phys. Rev. Lett. **99**, 114503 (2007).